Sensors and Materials, Vol. 17, No. 4 (2005) 179–186
MYU Tokyo

S & M 0596

Characterization of Orientation-Dependent Etching Properties of Quartz: Application to 3-D Micromachining Simulation System

Di Cheng*, Kazuo Sato, Mitsuhiro Shikida, Atsushi Ono[1], Kenji Sato[1]
Kazuo Asaumi[2] and Yasuroh Iriye[2]

Department of Micro-Nano Systems Engineering, Nagoya University
Furo-cho, Chikusa-ku, Nagoya, 464-8603, Japan
[1]Toyo Communication Equipment Co., Ltd.
[2]Fuji Research Institute Corporation

(Received Ocober 1, 2004; accepted March 17, 2005)

Key words: anisotropic etching, orientation dependence, ammonium bifluoride, single-crystal alpha-quartz

Novel characterization results of anisotropic etching properties of single-crystal alpha-quartz for a number of orientations using a spherical specimen are reported. The dimensions of the specimen's surface were measured before and after etching, and the changes were used to calculate the etching rates for a single etching operation for a number of orientations. The etching rates were high at the Z-axis, but not the highest. Low etching rates, sometimes close to zero, were measured for directions perpendicular to the Z-axis. We first report the etching rate distribution perpendicular to the Z-axis. The estimated etching rates further allow us to simulate complete three-dimensional etching for arbitrarily oriented quartz wafers.

1. Introduction

Quartz is a material that can be micromachined using orientation-dependent etching with an NH_4HF_2 (ammonium bifluoride) saturated solution. The etching process is represented by the following formula.(1)

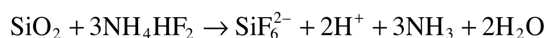

$$SiO_2 + 3NH_4HF_2 \rightarrow SiF_6^{2-} + 2H^+ + 3NH_3 + 2H_2O$$

The anisotropic etching of alpha-quartz has been widely used, for example, to fabricate microstructures such as quartz temperature sensors(2) and miniature quartz tuning fork resonators for wristwatches.(3) However, the anisotropy in the etching rate is less clear than

*Corresponding author, e-mail address: chengdi@kaz.mech.nagoya-u.ac.jp

that for silicon, which can also be etched anisotropically.[4–7] No systematic studies of the anisotropic etching of alpha-quartz had been reported until Ueda[8] reported the measured anisotropy in etching by using quartz wafers with 21 different cut angles. However, there is still an insufficient amount of reported data to analyze the etching profile of quartz. We have now characterized the anisotropic etching properties of quartz by applying a method previously developed for characterizing silicon etching.[4,6,7]

We characterized the anisotropic etching properties of silicon by using a hemispherical single-crystal specimen and estimating the etching rate for a number of orientations from the change in surface profile. Due to the difference in the crystal system between silicon and quartz (silicon has a tetragonal and quartz has a hexagonal system, as shown in Fig. 1), a hemispherical specimen does not cover all the orientations possible with quartz. To overcome this problem, we used a spherical specimen made of alpha-quartz. A photograph of it is shown in Fig. 2, and a cross section is shown in Fig. 3.

Because quartz has a significantly different crystal system than silicon (see Fig. 1(a)), expressing the orientations using the normal Miller index is difficult. For example, the crystal properties of the a1- and a2-axis directions are physically identical, but with the Miller index they are expressed as [110] and [100]. Therefore, when expressing a hexagonal crystal system such as quartz or Zn, one usually uses a special index, the Miller-Bravais index. As shown in Fig. 1(a), there are four axes in a hexagonal system crystal structure: three axes (a1, a2, and a3) on one base plane meet at angles of 120°, and the other axis (Z) is perpendicular to this plane. This crystal structure is represented accurately by the Miller-Bravais index because it has four parameters (*hkil*) corresponding to the four axes.

The principal crystal planes of alpha-quartz after crystal growth are shown in Fig. 1(b). Some orientations have idiomatic names, *e.g. m*: $\{10\bar{1}0\}$; *R*: $(10\bar{1}1)$, $(\bar{1}101)$, $(0\bar{1}11)$; and *r*:

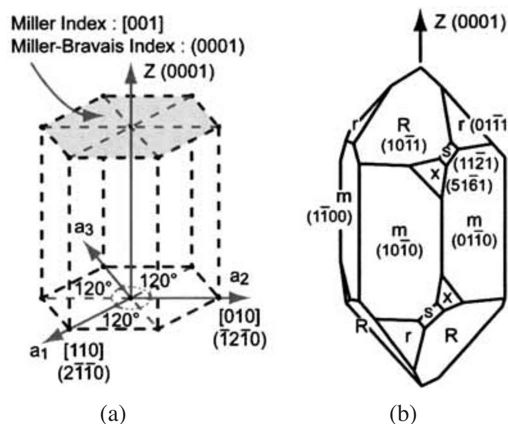

(a) (b)

Fig. 1. Hexagonal system crystal structure of quartz and Miller-Bravais index: (a) lattice directions of quartz; (b) some crystal planes after crystal growth.

Fig. 2. Spherical single-crystal alpha-quartz specimen with Cr and Au films protecting the orientation-flat and bottom surface.

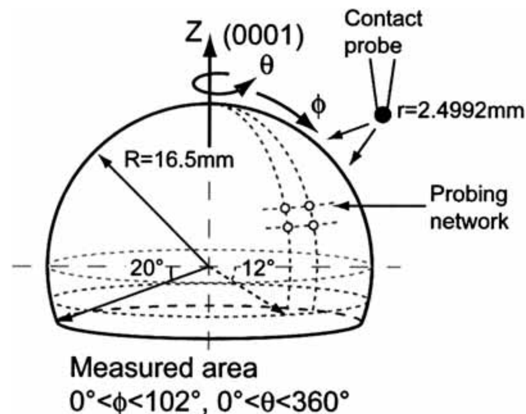

Fig. 3. Cross section of spherical specimen made of alpha-quartz.

$(\bar{1}011)$, $(1\bar{1}01)$, $(01\bar{1}1)$. In this work we will refer to the “equator” as the set of directions perpendicular to the Z-axis, including the m planes. The fastest crystal growth has an orientation of (0001), suggesting that etching may be the fastest at this orientation.

2. Experimental

The single-crystal quartz spherical specimen (cross section shown in Fig. 3) was mechanically ground, lapped, and polished into a mirrored surface with a radius of 16.5 mm. The top of the hemisphere was oriented towards (0001), and it had an orientation-flat at the periphery oriented towards $(\bar{1}2\bar{1}0)$. The orientation-flat and bottom surface were protected against etching by Cr and Au films with thicknesses of 300 Å for Cr and 1625 Å for Au, because the flat and bottom surface were used as coordinate origins when we

compared the surfaces before and after etching.

Using a spherical specimen enabled us to obtain the etching rates for all crystallographic orientations under the same etching conditions simultaneously. The etching rate ratios obtained for different orientations are thus reliable. We were also able to evaluate the surface roughness for all the orientations after etching for exactly the same time.

We calculated the etching rates based on the change in the surface profile of the specimen, which was determined by measuring the surface profile before and after etching using a UPMC550CARAT three-dimensional surface-measuring machine (Carl Zeiss Co., Ltd.) having a mechanical contact probe. As shown in Fig. 3, the surface profile was probed every 2°, both in latitude (–12 to +90°) and longitude (0 to 358°). The total number of probe points was 9360.

2.1 *Effect of etching depth of the hemisphere*

With a spherical specimen, the etching rates can be evaluated more accurately when the etching depth and time are as large as possible. However, as etching is advanced, the specimen surface is removed, eventually leading to a polygonal profile. As a result, some orientations are lost from the surface and the corresponding etching rates cannot be estimated. In the example shown in Fig. 4, A and B are neighboring points on a spherical specimen and have different crystallographic orientations. The R is the radius of the hemisphere, ε_1 and ε_2 are the etching depths of points A and B, respectively, and A' and B' are the positions of the surface after etching starting from A and B, respectively.

Since no interference between contiguous orientations A' and B' is desired after etching, the following relationship must be satisfied:

$$\frac{|\varepsilon_1 - \varepsilon_2|}{R} < (1 - \cos\theta). \tag{1}$$

In our case, R is 16.5 mm, and the probing density θ is 2°. Substituting these values into eq. (1), we get the admissive etching depth difference between A and B, estimated to be 100

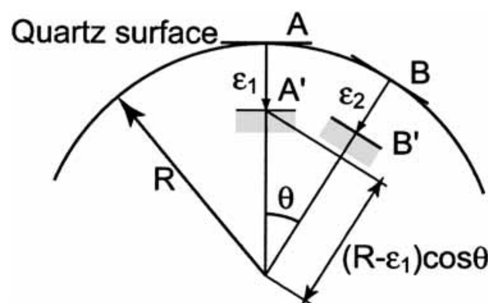

Fig. 4. Geometrical conditions under which two contiguous orientations ingerfere with each other after etching, related to the desity of the probing network. ε_1, ε_2: Etching depth. θ: Unit angle of probing network.

μm. This means we can etch the surface to a depth of 100 μm without causing interference among orientations.

2.2 *Etching conditions and processes*

We used an NH_4HF_2 (ammonium bifluoride) saturated solution as an etchant, and the etching temperatures were selected as 70°C and 80°C. The etching steps were as follows:

1. Protect the orientation flat and bottom surface with Cr and Au films. Film thicknesses are 300 Å for Cr and 1625 Å for Au.
2. 3-D form measurement before etching.
3. Etch in NH_4HF_2 saturated solution (at 70°C and 80°C).
4. 3-D form measurement after etching.
5. Calculate the etching rate and correct the data.

3. Results and Discussion

3.1 *Orientation dependence in etching rate*

An example contour map of the etching rate for an etching temperature of 70°C is shown in Fig. 5. It shows that the etching rate of quartz has three-fold symmetry about the (0001) axis. While the (0001) orientation exhibited a high etching rate, the rate was not the highest. Low etching rates occurred along the equator, even as low as close to zero. This means that a (0001) wafer can be etched perpendicular to the wafer surface by wet etching with minimal side-etching in the same manner as with deep RIE.

As shown in Table 1, the etching rate of the single-crystal quartz depended greatly on the temperature. A difference of only 10°C changed the etching rate about 2.2 times.

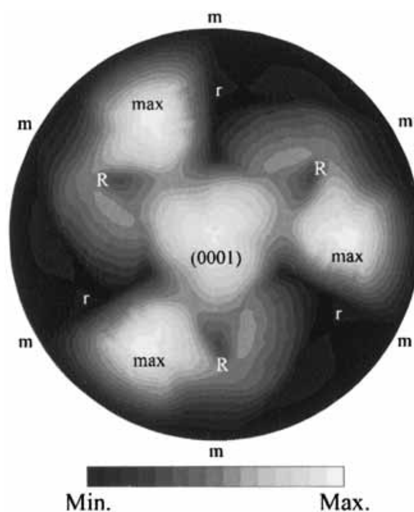

Fig. 5. Etching-rate contour map (etching temperture of 70°C).

Table 1
Etching rates of a number of crystallographic orientations at etching temperatures of 70 and 80°C. In parentheses are normalized values relative to (0001) orientation.

Crystallographic orientation	Etching rates (μm/min)	
	70°C	80°C
(0001)Z	0.571(1.00)	1.261(1.000)
$(\bar{1}2\bar{1}2)$	0.565(0.99)	1.270(1.01)
$(\bar{1}2\bar{1}0)$	0.013(0.02)	0.032(0.03)
$(\bar{1}102)$	0.347(0.61)	0.755(0.60)
$(\bar{1}101)$R	0.242(0.42)	0.608(0.48)
$(\bar{1}100)$m(Min.)	0.002(<0.01)	0.003(<0.01)
$(\bar{2}112)$	0.256(0.45)	0.631(0.50)
$(\bar{2}111)$s	0.512(0.90)	1.177(.93)
$(\bar{2}110)$	0.043(0.08)	0.094(0.08)
$(51\bar{6}1)$x	0.054(0.09)	0.116(0.09)
$(\bar{1}012)$	0.120(0.21)	0.297(0.24)
$(\bar{1}011)$r	0.059(0.10)	0.143(0.11)
$(\bar{2}4\bar{2}3)$Max.	0.590(1.03)	1.432(1.14)

3.2 *Etching rates along the equator*

As mentioned above, with a spherical specimen, the etching rate can be more accurately estimated when the etching depth and time are as large as possible. However, along the equator, there were orientations having extremely low etching rates. Some orientations even had an etching rate near zero, making it difficult to obtain the exact etching rates of those orientations using only a spherical specimen. To overcome this problem, we also prepared a number of chip specimens having orientations along the equator and etched them under the same conditions used for the spherical specimen.

An etching rate distribution map along the equator measured using the spherical specimen and chip specimens is shown in Fig. 6. Major and minor peaks appeared every 120°. Note that, even in the case of the major peaks, the etching rates were very low. The rates did not differ much between the spherical specimen and the chip specimens. The results for the chip specimens should be more reliable for these orientations, as they were able to be etched deeper for longer times. We thus used the data for the chip specimens to increase the accuracy of the etching rates in the database.

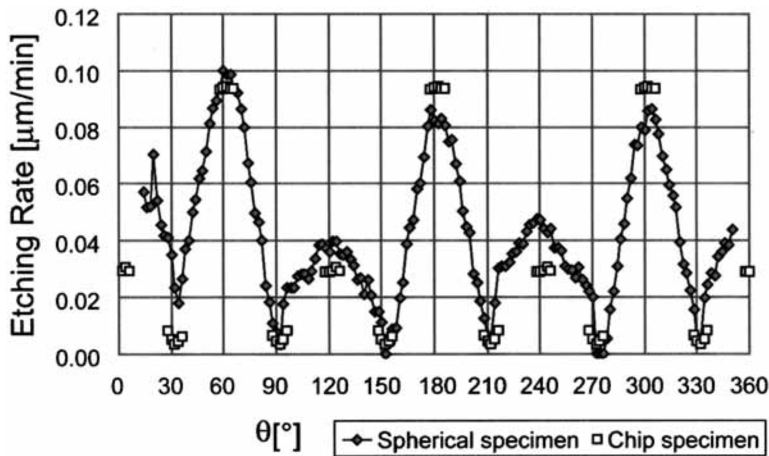

Fig. 6. Etching rate distribution along equator compared with rates measured using chip specimens.

4. 3-D Micromachining Simulation System

Using the database of etching rates, along with the previously developed anisotropic etching process simulation system (MICROCAD),[4,6,7] we can now predict the three-dimensional etching profiles of quartz wafers. The etching simulation of a selectively masked (0001) quartz wafer is illustrated in Fig. 7. The concave and convex profiles were analyzed by applying both hole- and island-shaped mask patterns. We obtained a well-defined cube with minimal side-etching. By using the MICROCAD system, we can predict the etching results before actual processing. In addition, by linking the simulation system with the etching rate database, we can minimize the time needed to develop fabrication processes.

5. Conclusion

We measured the etching rate of single-crystal alpha-quartz as a function of the crystallographic orientation using a spherical specimen. The orientation-dependent etching rate in ammonium bifluoride saturated solution was estimated for a dense net of orientations. The etching rates along the equator were very low; some were even close to zero. Since quartz has excellent anisotropy during wet etching, it can be processed with minimal side-etching. It is thus now possible to simulate the micromachining features of quartz during anisotropic wet etching.

This research has clarified in detail the etching properties of quartz in terms of orientation and temperature dependence.

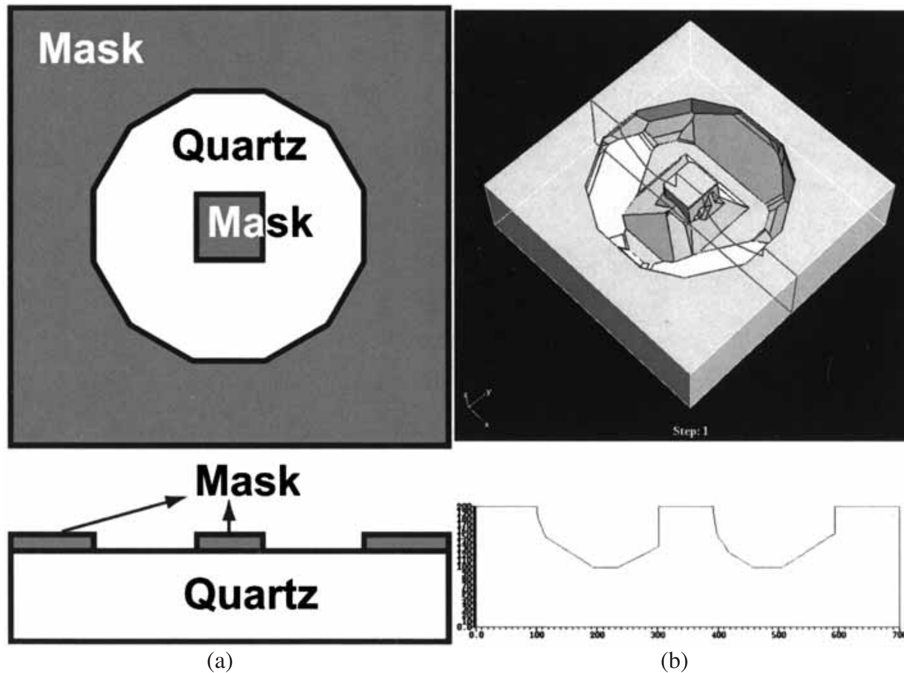

Fig. 7. Anisotrpic etching simulation of quartz crystal based on etching rate diagram (hole and island pattern) with temperature of 80°C and etching time of 60 min. (a) Mask area; (b) 3-D simulation results and cross-sectional view.

Acknowledgements

This work was supported by a grant-in-aid for Scientific Research (A) No 14205016 from the JSPS. It was also supported by the 21st COE Program (Micro- and Nano-Mechatronics for Information-Based Society).

References

1 J. Yoshimura and S. Taki: Original report of Faculty of Engineering Yamanashi University **31** (1980) 154.
2 T. Ueda, F. Kohsaka, T. Iino and D. Yamazaki: T-SICE **23** (1986) 1117. (in Japanese)
3 J. H. Staudte: Proc. of the 27th annual symposium on frequency control (1973) p. 50.
4 K. Sato, M. Shikida, Y. Matsushima, T. Yamashiro, K. Asaumi, Y. Iriye and M. Yamamoto: Sensors and Actuators A **64** (1998) 87.
5 O. Powell and H. B. Harrison: J. Micromech. Microeng. **11** (2001) 217.
6 K. Sato, M. Shikida, T. Yamashiro, K. Asaumi, Y. Iriye and M. Yamamoto: Sensors and Actuators A **73** (1999) 131.
7 K. Asaumi, Y. Iriye and K. Sato: Proc. of IEEE Micro Electro Mechanical Systems (MEMS) Workshop (Nagoya, 1997) p. 412.
8 T. Ueda, F. Kohsaka, T. Iino and D. Yamazaki: T-SICE **23** (1986) 1233. (in Japanese)